Received 16 February 2020; revised 28 April 2020; accepted 4 May 2020. Date of publication 6 May 2020; date of current version 22 May 2020.
The review of this article was arranged by Editor C. C. McAndrew.

Digital Object Identifier 10.1109/JEDS.2020.2992798

RESURF Principle in AlGaN/GaN HEMTs: Accurate 1-D Modeling on Off-State Avalanche Breakdown Behavior via Effective Concentration Profile

JUN ZHANG [1,2,3] (Member, IEEE), AND YUFENG GUO [1,2] (Member, IEEE)

1 College of Electronic and Optical Engineering, Nanjing University of Posts and Telecommunications, Nanjing 210046, China
2 National and Local Joint Engineering Laboratory for RF Integration and Micro-Packaging Technologies, Nanjing University of Posts and Telecommunications, Nanjing 210046, China
3 State Key Laboratory of Electronic Thin Films and Integrated Devices, University of Electronic Science and Technology of China, Chengdu 610054, China

CORRESPONDING AUTHOR: Y. GUO (e-mail: yfguo@njupt.edu.cn)

This work was supported in part by the China Post-Doctoral Science Foundation under Grant 2018M642291, in part by the Natural Science Foundation of Jiangsu Province under Grant BK20190237, in part by the Opening Project of State Key Laboratory of Electronic Thin Films and Integrated Devices under Grant KFJJ201907, and in part by the National Natural Science Foundation of China under Grant 6190030245, Grant 61574081, and Grant 61874059.

ABSTRACT We present a simple but accurate 1-D methodology of modeling for AlGaN/GaN High Electron Mobility Transistors (HEMTs), and by which means study its Reduced Surface Field (RESURF) effect. By using the Effective Concentration Profile Concept, the proposed methodology accounts the interactions between each layer and electric field crowding induced by gate/drain electrodes simultaneously without introducing any simulation results and correction factors. The proposed model indicates that same as that in silicon-based lateral power devices, the RESURF effect is also present in AlGaN/GaN HEMTs. Thus, the channel layer doping of AlGaN/GaN HEMTs plays a leading role in determining the devices' off-state characteristics. Owing to the veracity and simplicity of the proposed model, in this paper, the devices' breakdown voltage and RESURF criterion are analytically obtained via a 1-D approach for the first time. The good agreements between the analytical model, experimental results, and 2-D simulations verify the validity of the proposed methodology.

INDEX TERMS AlGaN/GaN HEMTs, RESURF principle, 1-D analytical model, breakdown voltage.

I. INTRODUCTION

The most notable feature of power devices is the ability to block high voltage when operates in off-state [1]–[6]. Due to the polarization-induced free carriers and wide-bandgap that gallium nitride material has, the GaN-based transistor benefits from its excellent electron transport capability and high breakdown voltage making it favorable in the power semiconductor realm [1]–[4], [7]. Much effort has been devoted to the developing of new device structures to meet the unceasing demand for reducing the On-Resistance (Ron) and keeping a high breakdown voltage (BV) [7]–[10]. Among them, the most direct method is to introduce the pre-existing techniques that originally applied to silicon-based power devices into the AlGaN/GaN High Electron Mobility Transistors (HEMTs) [1]–[3], [11]. By using the carefully designed structure parameters, these techniques enable power devices to achieve a better off-state characteristic via reshaping the electric field [5]–[6], [12]–[14]. These breakdown techniques are mostly considered as an improvement on the basis of the Reduced Surface Field (RESURF) technique. However, the application and optimization of these techniques on GaN-based devices are limited and difficult due to the lack of effective physics-based analysis. What's more, the researches on AlGaN/GaN HEMTs at present are mostly conducted through simulation tools or experiments [7]–[14]. The structure optimization is almost impossible as both these approaches are time-consuming and costly. Therefore, despite over two decades of development, some rather ubiquitous features of the breakdown mechanism of AlGaN/GaN HEMTs are still not well understood. One

This work is licensed under a Creative Commons Attribution 4.0 License. For more information, see https://creativecommons.org/licenses/by/4.0/

primary example is the relations between impurities dose, depletion, and breakdown voltage [13]–[15].

Understanding the off-state breakdown behavior in AlGaN/GaN HEMTs is of crucial importance to design and realize better techniques and to improve device performance. Due to the sophisticated nature and stacked vertical structure of AlGaN/GaN HEMTs, to date, analytical models are established by solving 2-D Poisson's equation and the introduction of artificial correction factors or even simulation results are usually required [13]–[17]. Moreover, due to the distinctive structure of AlGaN/GaN HEMTs, the electric field crowding inevitably appears near the Drain and Gate electrodes. Such a curvature-induced effect further adds the modeling difficulty due to its irregular boundary conditions. To avoid such difficulties, to date analytical models are usually only focusing on the structure employed field plates [13]–[16]. The particularity of these 2-D methods limits their application scenarios.

In this paper, a general-purpose 1-D modeling approach is proposed to explore the off-state performance of AlGaN/GaN HEMTs with the help of the Effective Concentration Profile Concept. So that the electric field profile and BV can be obtained by solving 1-D Poisson's equation which greatly drops the analysis difficulties. The proposed 1-D model not only can depict the off-state characteristic of AlGaN/GaN HEMTs but also indicates that the GaN-channel layer doping dose ($Q_{ch} = N_{ch} \times t_{ch}$) takes a significant role in optimizing the device's off-state breakdown behavior. The effectiveness and correctness of the proposed methodology are well verified by the good comparison between 2-D simulation results obtained by Sentaurus, a Synopsys technology computer-aided design (TCAD) tool, experimental results, and analytical results obtained by the proposed model. The physics model and math setting used for simulation are in accordance with Sentaurus Workbench template. The use of this Effective Concentration Profile (ECP) concept that originally proposed for silicon-based power devices on the modeling of GaN-based HEMTs, and with its outcomes achieve a good agreement between modeled, simulated and measured results further prove the universality and effectiveness of the proposed methodology in exploring the off-state breakdown characteristics of lateral power devices.

II. MODELING METHODOLOGY

A typical AlGaN/GaN HEMT is constituted by a stacked structure which from top to bottom is Si_3N_4 passivation layer, AlGaN barrier layer, GaN channel layer, GaN buffer layer, and substrate [1], [2], [7]–[10]. As shown in Fig. 1 (a), for the modeling and simulation simplicity, a depletion-model (D-model) device structure is adopted in this paper. Hence, a negative gate voltage is employed to maintain the off-state in simulations. As shown in Fig. 1 (b), when the device operates on off-state, the depletion region forms both laterally and vertically to sustain the applied voltage. The potential function in each layer satisfies the 2-D Poisson's

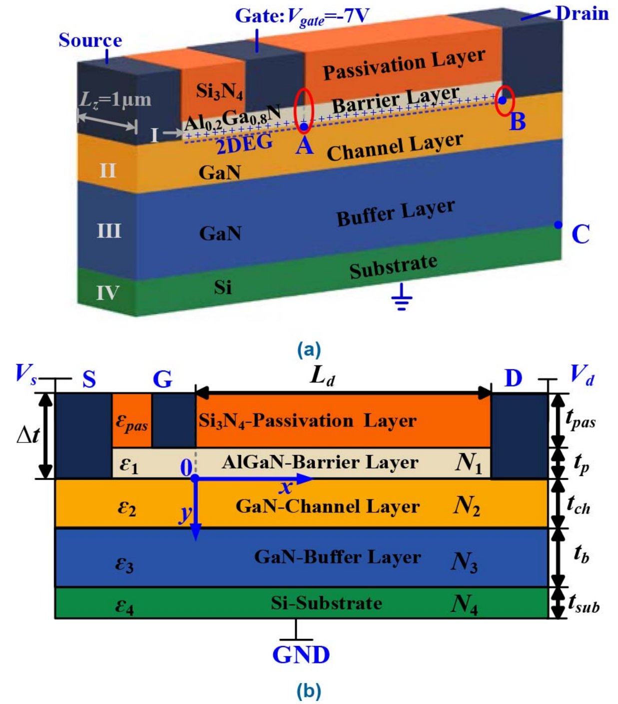

FIGURE 1. (a). 3-D view of the AlGaN/GaN HEMT and (b). 2-D cross-section of the AlGaN/GaN HEMT with silicon substrate for modeling (x-y plane).

equation, which yields:

$$\frac{\partial^2 \varphi_i(x, y)}{\partial x^2} + \frac{\partial^2 \varphi_i(x, y)}{\partial y^2} = -\frac{qN_i}{\varepsilon_i}, \quad i = 1, 2, 3, 4 \tag{1}$$

where the ε_i and N_i are the dielectric constant and doping concentration of each layer, respectively. In this paper, if not otherwise stated, the intrinsic background carrier concentration of the channel layer is $N_{ch0} = 1 \times 10^{15}\text{cm}^{-3}$. To solving Eq. (1), a set of boundary conditions is required. In this paper, to simplify the derivation process as much as possible, a mathematical transformation ought to be applied. Thus, the influence of impurities (or part of them) on 2-D Poisson's equation can be equivalent to an extra boundary condition. Hence, in this case, the influence caused by the polarization charge at the AlGaN/GaN interface can be transformed into a virtual boundary condition, which yields:

$$\varphi_1\left(x, -t_p\right) = -V_{2DEG} = -qQ_e\frac{t_p}{\varepsilon_1} \tag{2}$$

where Q_e is the polarization charge density whom a strong function of Al composition x in the AlGaN material. Based on the polarization effect theory, the polarization charge density in this paper is determined by:

$$Q_e = |P_{PE}(Al_xGa_{1-x}N) + P_{SP}(Al_xGa_{1-x}N) - P_{SP}(GaN)| \tag{3}$$

where P_{PE} and P_{SP} are the piezoelectric and spontaneous polarization charge density, respectively. In this paper, the Al composition in the AlGaN material is 0.2. Thus, for simplicity, the $Q_e = 1.0 \times 10^{13}\text{cm}^{-2}$. Therefore, the upper and

lower boundary conditions of each layer can be obtained by using electric displacement and electric potential continuous conditions at both its interfaces. The boundary conditions at the top and bottom of the device satisfy:

$$\left.\frac{\partial\varphi_1(x,y)}{\partial y}\right|_{y=-(t_p+t_{pas})} = \left.\frac{\partial\varphi_4(x,y)}{\partial y}\right|_{y=t_{ch}+t_b+t_{sub}} = 0 \quad (4)$$

So far, the boundary conditions for modeling are obtained properly. The effect of two-dimensional electron gas (2DEG) on channel potential is equivalent to a virtual potential on the surface of barrier layer. By submitting electric displacement and potential continuous conditions, into Eq. (2) and Eq. (1), a general differential equation for the potential distribution function of each layer can be obtained. Since the lateral breakdown occurs at the AlGaN/GaN heterojunction, the breakdown characteristic of the GaN channel layer is in great importance. Accordingly, its surface electric potential can be expressed as:

$$\frac{\partial^2\varphi_2(x,0)}{\partial x^2} - \frac{\varphi_2(x,0)}{t^2} = -\left(\frac{qN_2}{\varepsilon_2} - \frac{qN_3}{\varepsilon_3}\right)\left(\frac{K_{34}t_{sub}t_b + t_b^2}{2t^2}\right) - \frac{qN_1}{\varepsilon_1}\left(\frac{K_{14}t_{sub}t_p + t_p^2}{2t^2}\right) + \left(\frac{V_{2DEG}}{t_{pas}}\right) \times \left(\frac{K_{14}t_{sub} + 2t_p + 2K_{12}t_{ch} + 2K_{13}t_b}{2t^2}\right) \quad (5)$$

where $K_{ij} = \varepsilon_i/\varepsilon_j$ represents the dielectric constant ratio of layer i and j, $t = [0.5(t_b + t_{ch})^2 + 0.5K_{34}t_{sub}\ (t_b + t_{ch})]^{0.5}$ is the characteristic thickness of the stacked vertical structure, t_{pas}, t_p, t_{ch}, t_b and t_{sub} being the thickness of passivation layer, barrier layer, channel layer, buffer layer, and substrate depletion region, respectively. A more detailed derivation process of Eq. (5) is provided in the Appendix for reference. Furthermore, due to rigorousness in mathematical derivation, the proposed method can also be applicable to the AlGaN/GaN HEMTs with field plates in theory. The channel layer between the gate and drain region is the main structure that sustains reverse-applied voltage in the lateral. In this paper, for simplicity, such a region is considered as a drift region that has the length of L_d and thickness of t_{ch}. Especially, since the AlGaN barrier layer is usually a very thin layer ($t_p = 3 - 20$nm in this paper), its doping and thickness have a trivial impact in Eq. (5). Thus, the N_1 and t_p are therefore neglected in subsequent modeling and discussions. By applying the Effective Concentration Profile Concept to Eq. (5), The ECP that indicates the influence of stacked structure and applied voltage can be obtained, which yields [4], [6], [12], [18]:

$$N_{coup}(x) = N_{de}\left[\left(\frac{x}{L_d}\right)^a + \left(\frac{L_d - x}{L_d}\right)^a\right] - \frac{2\varepsilon_2 V_d}{qt^2}\left(\frac{x}{L_d}\right)^a \quad (6)$$

where $a = 2L_d/t$ being the drift region shape factor, N_{de} indicates the influence of stacked structure, especially the 2DEG, on ECP, which yields:

$$N_{de} = (N_2 - K_{23}N_3)\left(\frac{K_{34}t_{sub}t_b + t_b^2}{2t^2}\right) + \left(\frac{\varepsilon_2 V_{2DEG}}{qt_{pas}}\right)\left(\frac{K_{14}t_{sub} + 2K_{12}t_{ch} + 2K_{13}t_b}{2t^2}\right) \quad (7)$$

It is worth to be noted that due to the deep-level impurities that within, the buffer layer, in fact, behaves as a P-type region [16], [17]. Accordingly, the N_3 being the equivalent P-type doping concentration that induced by impurities and traps. In this paper, for simplicity, intrinsic background carrier concentration of the buffer layer satisfies $N_3 = 5.0 \times 10^{13}\text{cm}^{-3}$. Meanwhile, in this work, the passivation layer and substrate layer are defaults as $t_{pas} = 0.2\mu$m, $P_{sub} = 2.0 \times 10^{14}\text{cm}^{-3}$. Moreover, as shown in Fig. 1 (a), the right angle of the gate and drain electrodes induces intense electric field crowding which shall significantly reshape the electric field profile in the channel layer, especially the areas near point A and B. By employing the similar method that reported in REF [6], the equivalent curvature effect induced ECP increment can be given as:

$$N_{crow}(x) = \frac{\varepsilon_2}{q}\left[\frac{E_2(L_d,0)}{2} \cdot \frac{\Delta t}{(L_d + \Delta t - x)^2} - \frac{E_2(0,0)}{2} \times \frac{\Delta t}{(x + \Delta t)^2}\right] \quad (8)$$

where $\Delta t = (t_{pas} + t_p)$ being the approximate radius of curvature, $E_2(0,0)$, $E_2(L_d,0)$ is the surface electric field peak at $x = 0$ and L_d, respectively. As point A and B in Fig. 1 (a) that shows, the lateral breakdown may occur at the two ends of the drift region on the surface. Such method reckons the right angle of the electrodes as a ring-like region for modeling simplicity. Apparently, this approximation is not mathematically rigorous. Nevertheless, the proposed method is proven to be accurate and effective [6]. Therefore, since the sophisticated 2-D structure is equivalent to a 1-D graded junction, thus the overall ECP of the GaN channel layer (N_{eff}) in an AlGaN/GaN HEMT can be obtained by using the semiconductor compensation principle, namely summing Eq. (7) and (8), which yields:

$$N_{eff}(x) = N_{coup}(x) + N_{crow}(x) \quad (9)$$

By using the proposed method, when considering other effects or structures (such as field plates), the model is still valid. In which case the overall impact of different effects on devices' off-state breakdown characteristics can be easily considered by simply adding the effective doping concentration increments of each effect to Eq. (9) [6]. However, the field plate structure is not considered in this paper. So far, by using N_{eff}, the influence of stacked structure, 2DEG and electrode-induced crowding effect are converted to the variation of Effective Concentration Profile. Therefore, the surface electric field of channel layer ($E(x) = E_2(x,0)$) can

be easily obtained by simply using 1-D Poisson's equation:

$$E(x) = \frac{E(0)}{2}\left(\frac{\Delta t}{x+\Delta t}+1\right) + \frac{E(L_d)}{2}\left(\frac{\Delta t}{L_d+\Delta t-x}\right) - \frac{qN_{de}t}{2\varepsilon_2}\left[\left(\frac{x}{L_d}\right)^{a+1} - \left(\frac{L_d-x}{L_d}\right)^{a+1}+1\right] + \frac{V_d}{t}\left(\frac{x}{L_d}\right)^{a+1}. \quad (10)$$

III. VERIFICATION AND DISCUSSIONS

A. SURFACE ELECTRIC FIELD PROFILE

For the AlGaN/GaN HEMTs that shown in Fig. 1, three possible breakdown points are point A, B, and C. According to the physics of avalanche breakdown, once one electric field peak at point A, B, C reaches the critical field of breakdown, the onset of significant current flow occurs and avalanche breakdown happens. Among them, the electric field peaks at point A and B determine the lateral breakdown. To quantitatively and qualitatively explore the breakdown mechanism of AlGaN/GaN HEMTs and further provide designing guidance, the proper analysis on the surface electric field profile is in great importance. As shown in Fig. 2, the analytical and numerical surface electric field profile agrees well under various biases and structure parameters since both the electrode-induced field crowding and the whole stacked vertical structure are taken into the model's consideration. Although a limited range of applied voltage from 800V to 1400V is given in Fig. 2, the model is still accurate beyond this range as long as the full-depletion condition of the channel and buffer layer can be fulfilled.

As Fig. 2 (a) and (b) indicate, the surface electric field profile of GaN-channel layer is a strong function of its doping dose ($Q_{ch} = N_{ch} \times t_{ch}$). Same as that in silicon-based lateral power devices, the surface electric field peak near the Drain region raises and drops with the increasing and decreasing of doping dose, respectively. Namely, the Reduced Surfaced Electric Field (RESURF) principle is also in effect for AlGaN/GaN HEMTs. The electric field peaks at A and B are formed by the combined effect of RESURF effect, 2DEG, and electrode-induced field crowding. Especially, when the channel layer doping dose has a relative low value, it only has a limited influence on the surface electric field profile which can be understood by using Eq. (7). As Eq. (7) indicates, when the channel layer doping is lightly doped, the equivalent channel layer doping concentration (N_{de}) is mainly determined by 2DEG. Fig. 2 (c) and (d) indicate that the surface electric field as a function of drift region length and applied voltage shows the same regularity as silicon-based lateral power devices. Same as that in conventional silicon-based lateral power devices, by using the ECP concept, the 2-D drift region of the channel layer can be equivalent to a 1-D graded junction whose doping concentration is determined by Eq. (9). As shown in Fig. 3, as the device operates on off-state, the 2-D depletion between lateral and vertical direction results in an N(x)P(x)-type drift region. Hence, an NP-type 1-D equivalent structure is therefore formed creating a reverse-biased junction at both ends of drift region (equivalent PN junction and NN$^+$ junction) along with a forward-biased junction in between. Such

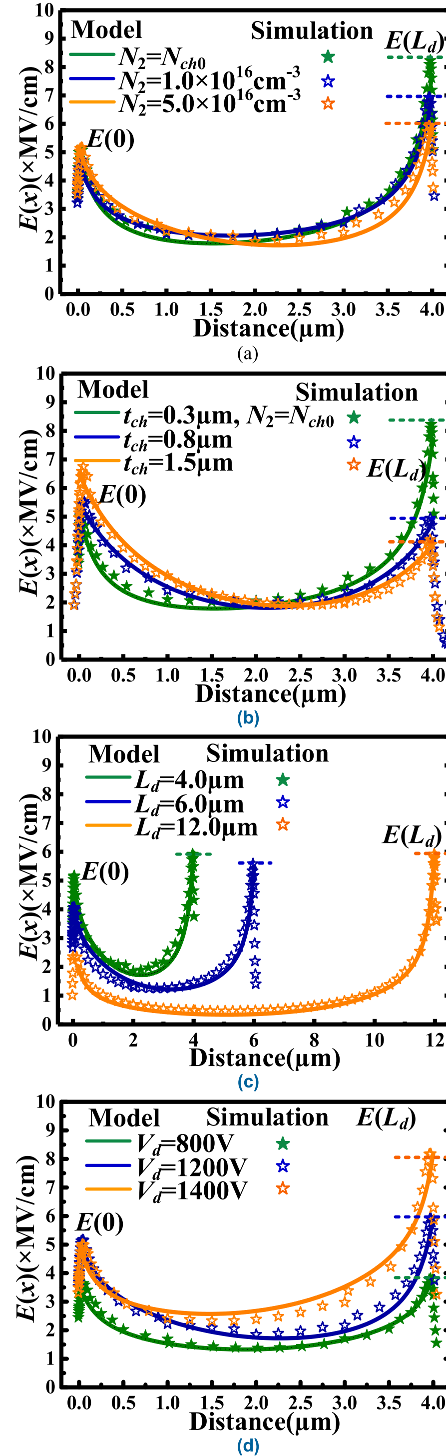

FIGURE 2. Simulated and calculated surface electric field profiles for various (a) Channel layer doping concentration (V_{app} = 1200V, t_{ch} = 0.3μm, L_d = 4.0μm), (b) Channel layer thickness (V_{app} = 1200V, N_2 = 1.0 × 10^{16}cm^{-3}, L_d = 4.0μm), (c) Drift region length (V_{app} = 1200V, N_2 = 5.0 × 10^{16}cm^{-3}, t_{ch} = 0.3μm), and (d) Applied drain voltage (N_2 = 1.0 × 10^{16}cm^{-3}, t_{ch} = 0.3μm, L_d = 4.0μm) with t_{pas} = 0.2μm, t_p = 0.02μm, $t_{ch} + t_b$ = 5.0μm, P_{sub} = 2.0 × 10^{14}cm^{-3}.

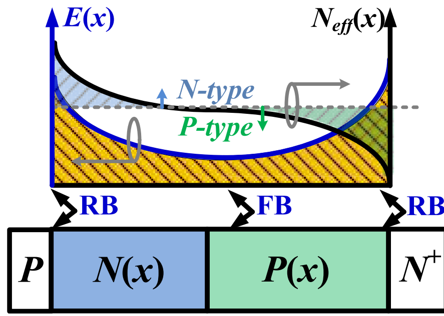

FIGURE 3. Effective lateral structure of channel layer and its electric field profile and Effective Concentration Profile. (RB: Reverse-Biased, FB: Forward-Biased).

an equivalent 1-D structure explained the basin-shaped surface electric field of the drift region in the channel layer [4], [5], [12].

B. BREAKDOWN VOLTAGE

As discussed above, the device's breakdown occurs when one of these three possible breakdown points reaches its critical electric field (E_C). Therefore, three possible breakdown location exists. Among them, the lateral full-depletion breakdown voltage can be obtained by submitting Eq. (10) into 1-D Poisson's equation, which yields:

$$BV_{lat}^{FPN} = \left(E_C L_d - \frac{qN_{de}t^2}{\varepsilon_2}\right)\left(\frac{L_d + \Delta t_{eff}}{t - \Delta t_{eff}}\right) \quad (11)$$

$$BV_{lat}^{FNN} = \left(E_C L_d + \frac{qN_{de}t^2}{\varepsilon_2}\right)\left(\frac{L_d + \Delta t_{eff}}{t + 2L_d + \Delta t_{eff}}\right) \quad (12)$$

where $\Delta t_{eff} = \Delta t \ln(L_d/\Delta t + 1)$ being the equivalent radius of curvature for the lateral depletion. The critical electric field of GaN(E_{CG}) and silicon (E_{CS}) material is determined by $E_{CG} = 4.0 \times 10^6$(V/cm) and $E_{CS} = 3.5 \times 10^4$(V/cm), respectively. According to the avalanche breakdown theory, when avalanche breakdown occurs, the impact ionization is a multiplicative phenomenon leading to a significant current flow through the depletion region. Therefore, when the breakdown condition has been fulfilled, the current rapidly increases with the increase of applied voltage. Meanwhile, the simulated/measured breakdown voltage is obtained under the condition when the leakage current reaches 1mA/mm. Thus, the deviation between the two methods of determining breakdown voltage is acceptable. Considering the charges induced by deep-level impurities, traps, etc., the E_{CG} used in this paper is much lower than the theoretical critical electric field of GaN. For the same reason, the derivation of vertical breakdown voltage is much more difficult as in which case the conventional assumption of 1-D planer junction no longer feasible. In fact, for the vertical structure, its electric field profile and breakdown mechanism has not been fully understood [14]–[17]. Especially, the experimental and theoretical analysis on the extra positive charges that in both the buffer layer and the buffer-substrate interface has not been presented yet. Therefore, we propose an empirical doping

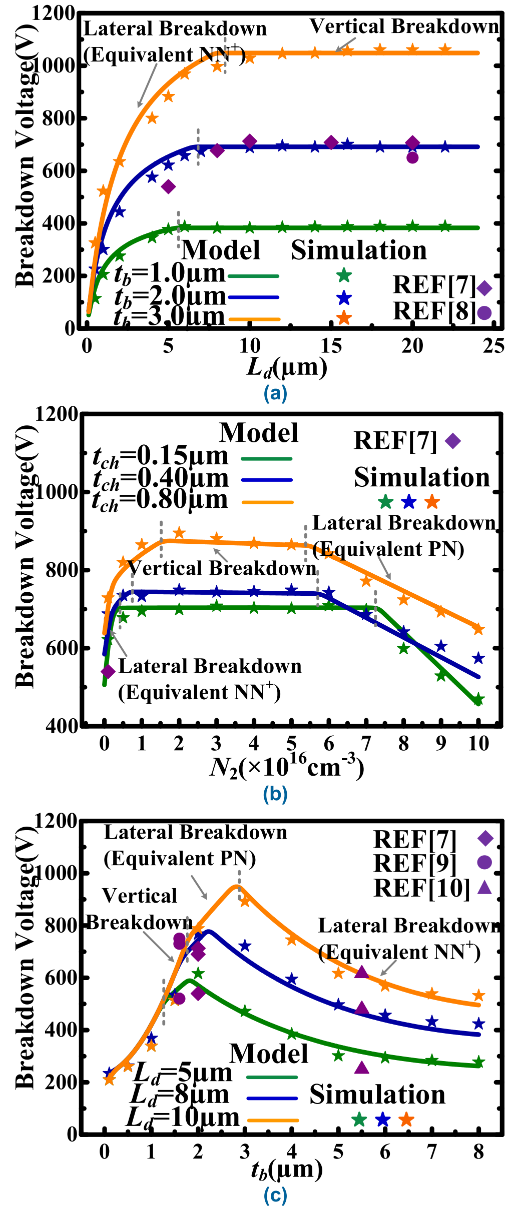

FIGURE 4. Simulated, calculated and measured breakdown voltage for various (a) Drift region length ($N_d = 1.0 \times 10^{15}$cm^{-3}, $t_{ch} = 0.15\mu$m, $t_p = 3.0$nm), (b) Channel layer doping concentration ($t_b = 2.0\mu$m, $t_p = 3.0$nm, $L_d = 5.0\mu$m), and (c) Buffer layer thickness ($N_2 = 1.0 \times 10^{15}$cm^{-3}, $t_{ch} = 0.15\mu$m, $t_p = 3.0$nm) with $t_{pas} = 0.2\mu$m, $P_{sub} = 2.0 \times 10^{14}$cm^{-3}.

dose $Q_{add} = 3 \times 10^{13}$cm^{-2} in the buffer layer. So that, as shown in Fig. 4, the analytically obtained vertical breakdown voltage can be well-matched with the experimental and 2-D TCAD simulation results in various devices parameters. Correspondingly, the breakdown voltage of the vertically stacked structure can be obtained by treating it as a conventional 1-D planer junction with extra charge Q_{add} in the buffer layer, which yields:

$$BV_{ver} = E_{CS}\left[K_{43}(t_b + t_{ch}) + \frac{t_{sub}}{2}\right]$$

$$-\frac{qN_2t_{ch}^2}{2\varepsilon_2}+\frac{q(N_3t_b+Q_{add})}{\varepsilon_2}(t_b+t_{ch}) \quad (13)$$

The substrate material, quality, and biases also have a considerable effect on the device vertical BV. The substrate layer mainly affects the vertical breakdown voltage of the device. Meanwhile, for a too thick buffer layer ($t_b > 20\mu$m), the buffer layer does not satisfy the full-depletion condition. In this case, the Eq (13) is no longer effective. In this paper, the defects in each layer and interface between different materials introduced in fabrication are considered by using deep-level impurities as traps during TCAD simulations. So far, the AlGaN/GaN HEMTs' lateral and vertical breakdown voltage has been analytically obtained using the proposed 1-D methodology. Thus, the breakdown voltage of the device can be easily determined by using the lowest between BV_{lat} and BV_{ver}, which yields:

$$BV = Min[BV_{lat}, BV_{ver}] \quad (14)$$

As shown in Fig. 4, the correctness and effectiveness of the proposed 1-D modeling method and simulation approach used in this paper are well-verified by the agreement between analytical, simulation and experimental results. The structural parameters for the modeled/simulated device and the devices in REF [7]–[10] are not exactly the same. The structure differences between each fabricated device and the modeled one contribute to the deviation between the measured and modeled results. Nevertheless, the consistency between modeled, simulated, experimental results, and the common trends of these independently obtained results verify the correctness of the proposed method. Worthy of note is that the simulations on AlGaN/GaN HEMTSs' breakdown voltage is very time-consuming. In this paper, the simulation results are obtained by the TCAD tool Sentaurus on a Linux server with 24-core 3.4 GHz CPU. To obtain the breakdown voltage under a set of specified structure parameters, the total CPU times of 9-24 hours and $12-17\times10^4$ mesh points are normally required. Not to mention the time costs generated by the convergence-related issues of the TCAD tool. The proposed methodology demonstrates its indispensable value as it can remarkably reduce time costs during the design phase [19]. Moreover, as Fig. 4 intuitively shows, the BV curves of GaN-based devices have a similar pattern as that in silicon-based lateral power devices [4]–[6], [13], [14], [18]. Namely, the existence of the RESURF effect in AlGaN/GaN HEMTs is theoretically validated for the first time by using the proposed 1-D ECP model.

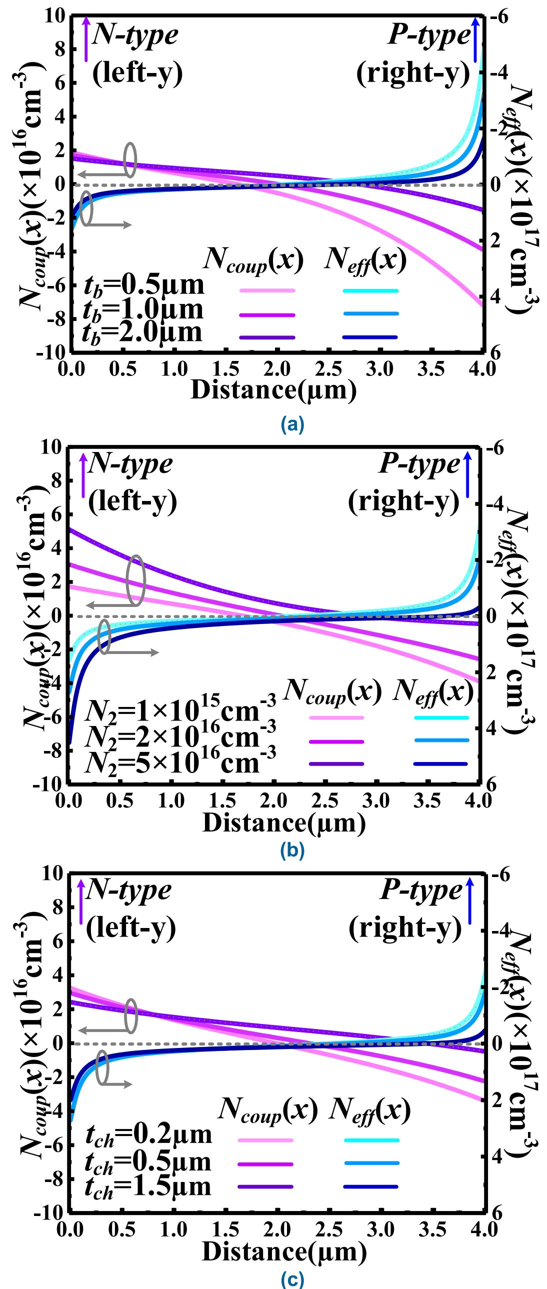

FIGURE 5. RESURF effect induced ECP($N_{coup}(x)$) and overall ECP($N_{eff}(x)$) for various (a) Buffer layer thickness ($N_d = 1.0\times10^{15}\mathrm{cm}^{-3}$, $t_{ch} = 0.4\mu$m, $t_p = 3.0$nm, $L_d = 4.0\mu$m), (b) Channel layer doping concentration ($t_b = 1.0\mu$m, $t_{ch} = 0.4\mu$m, $t_p = 3.0$nm, $L_d = 4.0\mu$m), and (c) Channel layer thickness ($N_d = 2.0\times10^{16}\mathrm{cm}^{-3}$, $t_b = 1.0\mu$m, $t_p = 3.0$nm, $L_d = 4.0\mu$m) with $t_{pas} = 0.2\mu$m, $P_{sub} = 2.0\times10^{14}\mathrm{cm}^{-3}$, $V_{app} = 400$V.

IV. RESURF EFFECT IN ALGAN/GAN HEMTS

The RESURF principle indicates that the reduction of the surface electric field became considerable when a strong 2-D coupling effect between the lateral and vertical depletion exists. The RESURF effect in GaN-based and Si-based devices differ widely in their relation to the structure parameters and the device's breakdown.

The RESURF effect induced ECP component ($N_{coup}(x)$) and overall ECP ($N_{eff}(x)$) vary widely against the actual doping concentration of the channel layer. As Fig. 5 clearly shows, the $N_{de} = N_{coup}(0)$ and $N_{eff}(0)$ are one and two orders of magnitude higher than N_2 respectively, thus further explaining the steep surface electric field profile of Fig. 2. As a result of the RESURF effect, the $N_{coup}(x)$ changes from equivalent N-type to P-type as x varies from 0 to L_d. The curvature effect, on the other hand, has a significant impact on enlarging the ECP near both ends of the drift region and

thus causing a boost in surface electric field peaks. Moreover, as Fig. 5 illustrates, to realize a high lateral breakdown voltage and avoid pre-mature breakdown caused by curvature effect, it is desirable to have the surface electric field be symmetric along the middle line of the drift region. Same as that in silicon-based lateral power devices, the $N_{coup}(x)$ ought to satisfies $N_{coup}(0) = -N_{coup}(L_d)$ and $N_{coup}(L_d/2) = 0$ when the lateral breakdown occurs. In which case, the lateral breakdown reaches its maximum, and the optimized N_{de_OPT} can be obtained by using Eq. (11) and (6), which yields:

$$N_{de_OPT} = \frac{\varepsilon_2 E_C L_d}{qt^2}\left(\frac{t-\Delta t_{eff}}{L_d+\Delta t}\right) \quad (15)$$

The correspondent maximum lateral breakdown voltage BV_{lat_MAX} can be also given by using Eq. (11), which yields:

$$BV_{lat_MAX} = E_C L_d\left(\frac{L_d+\Delta t_{eff}}{t-\Delta t_{eff}} - \frac{L_d+\Delta t_{eff}}{L_d+\Delta t}\right). \quad (16)$$

V. RESURF CRITERION

RESURF criterion is an optimization window to maximize the device's breakdown voltage, thus providing a crucial tool for designing [4]–[6], [18]. Same as that in silicon-based lateral power devices, the optimized drift region/channel layer effective doping dose($Q_{ch_OPT} = (N_2 - N_3) \times t_{ch}$) can be obtained by submitting Eq. (15) into Eq. (7), which yields:

$$Q_{ch_OPT} = \frac{2\varepsilon_2 E_C}{q}\left[\frac{(t-\Delta t_{eff})t_{ch}}{K_{34}t_{sub}t_b + t_b^2}\right] - \frac{2\varepsilon_2 V_{2DEG}}{qt_{pas}}\left[\frac{(t_{ch}+t_b)t_{ch}}{K_{34}t_{sub}t_b + t_b^2}\right] \quad (17)$$

Moreover, since the thickness of the depletion region in the substrate normally satisfies $t_{sub} = 2(t_{ch}+t_b)$, by submitting $E_{CG} = 4 \times 10^6$V/cm, $N_3 = 0$ and $Q_e = 1 \times 10^{13}$cm^{-2} into Eq. (17), a simplified RESURF criterion for the AlGaN/GaN HEMTs can be obtained as:

$$Q_{ch_OPT} = N_2 \times t_{ch} \le 1.6 \times 10^{13} \times (t_{ch}/t_b) cm^{-2} \quad (18)$$

Therefore, according to Eq.(18), the upper limit of the channel layer doping concentration can be given by:

$$N_{2_OPT} \le \frac{1.6 \times 10^{13}}{t_b} cm^{-3} \quad (19)$$

Obviously, as shown in Fig. 4, all the simulated and experimental results that the breakdown occurs at equivalent NN junction or vertical structure fall under this upper limit. Therefore, Eq. (18) and (19) provide a simple method to adjust channel layer doping dose/concentration, such a criterion ensures a considerable RESURF effect can be granted to achieve a desirable surface electric field.

VI. CONCLUSION

For the first time, in order to explore the RESURF effect of the AlGaN/GaN HEMTs and to provide effective and feasible guidance for the device's structural parameters designing, a novel 1-D analytical model is proposed in this paper using the Effective Concentration Profile concept. The proposed 1-D model converts the collective effects of structure parameters, 2DEG and electric field crowding on the device's BV characteristic to a superimposed ECP. Thus, a complicated 2-D problem with irregular boundary conditions can be easily analyzed by solving 1-D Poisson's equation. The correctness and effectiveness of the proposed 1-D ECP model are validated as the modeled results are found to be sufficiently accurate as compared both to TCAD simulation and to experimental results. Meanwhile, there are no fitting parameters used in the model. Due to the proper combination of the veracity and simplicity, for the first time, the proposed 1-D methodology provides a simple but accurate means to analyze devices' off-state breakdown characteristics. By using the proposed analytical model, the RESURF effect in AlGaN/GaN HEMTs is theoretically validated. Thus, a RESURF criterion is obtained for the first time, which provides a simple and effective tool for optimizing the structure parameters. Compare to the conventional TCAD tool, the proposed method has efficient accuracy and significant advantages in time and cost, thus may capable of reducing the designing cost.

APPENDIX

1. The mathematical derivation of a general differential equation for the surface potential of channel layer (Eq. (5)).

By using the Taylor series expansion on each semiconductor layer including AlGaN-barrier layer, GaN-channel layer, GaN buffer layer, and the silicon substrate layer, the electric potential in each layer can be given as:

Layer I: AlGaN-barrier layer: $(-t_p \le y \le 0)$

$$\varphi_1(x,y) = \varphi_1(x,-t_p) + \left.\frac{\partial\varphi_1(x,y)}{\partial y}\right|_{y=-t_p} \cdot (y+t_p) + \left.\frac{\partial^2\varphi_1(x,y)}{\partial y^2}\right|_{y=-t_p} \cdot \frac{(y+t_p)^2}{2} \quad (A1)$$

Layer II: GaN-channel layer: $(0 \le y \le t_{ch})$

$$\varphi_2(x,y) = \varphi_2(x,0) + \left.\frac{\partial\varphi_2(x,y)}{\partial y}\right|_{y=0} \cdot y + \left.\frac{\partial^2\varphi_2(x,y)}{\partial y^2}\right|_{y=0} \cdot \frac{y^2}{2} \quad (A2)$$

Layer III: GaN-buffer layer: $(t_{ch} \le y \le t_{ch}+t_b)$

$$\varphi_3(x,y) = \varphi_3(x,t_{ch}) + \left.\frac{\partial\varphi_3(x,y)}{\partial y}\right|_{y=t_{ch}} \cdot (y-t_{ch}) + \left.\frac{\partial^2\varphi_3(x,y)}{\partial y^2}\right|_{y=t_{ch}} \cdot \frac{(y-t_{ch})^2}{2} \quad (A3)$$

Layer IV: Si-substrate layer: $(t_{ch}+t_b \le y \le t_{ch}+t_b+t_{sub})$

$$\varphi_4(x,y) = \varphi_4(x,t_{ch}+t_b) + \left.\frac{\partial\varphi_4(x,y)}{\partial y}\right|_{y=t_{ch}+t_b} \cdot (y-t_{ch}-t_b) + \left.\frac{\partial^2\varphi_4(x,y)}{\partial y^2}\right|_{y=t_{ch}+t_b} \cdot \frac{(y-t_{ch}-t_b)^2}{2} \quad (A4)$$

The corresponding boundary conditions for each layer can be given by:

Layer I: The virtual boundary conditions:

$$\varphi_1(x, -t_p) = -V_{2DEG} = -qQ_e \frac{t_p}{\varepsilon_1} \tag{A5}$$

$$\left.\frac{\partial \varphi_1(x, y)}{\partial y}\right|_{y=-t_p} = \frac{V_{2DEG}}{t_{pas}} \tag{A6}$$

The electric potential continuous conditions:

$$\varepsilon_1 \left.\frac{\partial \varphi_1(x, y)}{\partial y}\right|_{y=0} = \varepsilon_2 \left.\frac{\partial \varphi_2(x, y)}{\partial y}\right|_{y=0}, \ \varphi_1(x, 0) = \varphi_2(x, 0) \tag{A7}$$

Here, although the passivation layer does have an electric field that exists within, when the device operates in off-state, the potential difference mainly exists between the Gate and Drain electrodes, namely in lateral direction. On the contrary, since no field plate structure is considered in this work, the actual (not virtual) vertical electric field that resulted in the potential difference between the upper and lower boundary of the passivation layer is ignorable. As long as no apparent vertical electric field exists in the passivation layer, the lateral electric field within the passivation layer won't have effects on the model and its derivation process. Moreover, the effects of interface defects of the gate ($x = 0$) and drain ($x = L_d$) on breakdown voltage can be considered by lowering the critical electric field. It is worthy to be noted that this approach to estimate the defects induced BV lowering is not mathematically rigorous. Yet, from the perspective of physics, this approach is reasonable. The good agreement between modeled, simulated, and experimental results also indicate the effectiveness of this estimation method.

Layer III:

$$\left.\frac{\partial \varphi_3(x, y)}{\partial y}\right|_{y=t_{ch}+t_b} = -K_{34} \frac{2}{t_{sub}} \varphi_3(x, t_b + t_{ch}) \tag{A8}$$

$$\varepsilon_2 \left.\frac{\partial \varphi_2(x, y)}{\partial y}\right|_{y=t_{ch}} = \varepsilon_3 \left.\frac{\partial \varphi_3(x, y)}{\partial y}\right|_{y=t_{ch}}, \ \varphi_2(x, t_{ch}) = \varphi_3(x, t_{ch}) \tag{A9}$$

Layer IV:

$$\left.\frac{\partial \varphi_4(x, y)}{\partial y}\right|_{y=t_{ch}+t_b+t_{sub}} = 0, \ \varphi_4(x, t_{ch} + t_b + t_{sub}) = 0 \tag{A10}$$

$$\varepsilon_3 \left.\frac{\partial \varphi_3(x, y)}{\partial y}\right|_{y=t_{ch}+t_b} = \varepsilon_4 \left.\frac{\partial \varphi_4(x, y)}{\partial y}\right|_{y=t_{ch}+t_b}, \quad \varphi_3(x, t_{ch} + t_b) = \varphi_4(x, t_{ch} + t_b) \tag{A11}$$

For the layer I and II, by subsisting Eq. (A1), Eq. (A6), Eq. (A7) to Eq. (1), the $\varphi_2(x,0)$ can be given as:

$$\varphi_2(x, 0) = \varphi_1(x, -t_p) + \frac{V_{2DEG}}{t_{pas}} \cdot t_p + \left.\frac{\partial^2 \varphi_1(x, y)}{\partial y^2}\right|_{y=-t_p} \cdot \frac{t_p^2}{2} \tag{A12}$$

$$\left.\frac{\partial \varphi_2(x, y)}{\partial y}\right|_{y=0} = K_{12} \frac{V_{2DEG}}{t_{pas}} + \left.\frac{\partial^2 \varphi_1(x, y)}{\partial y^2}\right|_{y=-t_p} \cdot K_{12} t_p \tag{A13}$$

The Eq. (A12) and (A13) can be therefore treated as two boundary conditions for the channel layer. For the layer II and III, by subsisting Eq. (A12) and (A13) to Eq. (A2) and Eq. (1), the $\varphi_3(x,0)$ can be given as:

$$\varphi_3(x, t_{ch}) = \varphi_1(x, -t_p) + \frac{V_{2DEG}}{t_{pas}} \cdot t_p + \left.\frac{\partial^2 \varphi_1(x, y)}{\partial y^2}\right|_{y=-t_p} \times \frac{t_p^2}{2} + \left(K_{12} \frac{V_{2DEG}}{t_{pas}} + \left.\frac{\partial^2 \varphi_1(x, y)}{\partial y^2}\right|_{y=-t_p} \cdot K_{12} t_p\right) t_{ch} + \left.\frac{\partial^2 \varphi_2(x, y)}{\partial y^2}\right|_{y=0} \cdot \frac{t_{ch}^2}{2} \tag{A14}$$

$$\left.\frac{\partial \varphi_3(x, y)}{\partial y}\right|_{y=0} = K_{13} \left(\frac{V_{2DEG}}{t_{pas}} + \left.\frac{\partial^2 \varphi_1(x, y)}{\partial y^2}\right|_{y=-t_p} \cdot t_p\right) + \left.\frac{\partial \varphi_2(x, y)}{\partial y}\right|_{y=0} \cdot t_{ch} \tag{A15}$$

Also, the Eq.(A14) and (A15) can be used as boundary conditions for the layer III and IV. Meanwhile, for the silicon substrate, its vertical depletion satisfies:

$$\left.\frac{\partial \varphi_4(x, y)}{\partial y}\right|_{y=t_{ch}+t_b} = \frac{qP_{sub}}{\varepsilon_s} \cdot t_{sub} \tag{A16}$$

For the layer III, by subsisting Eq. (A14), (A15), and (A16) to Eq. (1) and Eq. (A4), the $\varphi_3(x,y)$-related terms can be replaced by $\varphi_1(x,y)$ and $\varphi_2(x,y)$-related terms. Therefore, the Eq. (A14) can be further simplified, which yields:

$$\left.\frac{\partial^2 \varphi_2(x, y)}{\partial y^2}\right|_{y=0} = \left(\frac{qN_2}{\varepsilon_2} - \frac{qN_3}{\varepsilon_3}\right) \times \frac{\left(K_{34} t_{sub} t_b + t_b^2\right)}{\left[(t_b + t_{ch})^2 + K_{34} t_{sub}(t_b + t_{ch})\right]} - \left(\frac{V_{2DEG}}{t_{pas}}\right) \times \frac{\left(K_{14} t_{sub} + 2t_p + 2K_{12} t_{ch} + 2K_{13} t_b\right)}{\left[(t_b + t_{ch})^2 + K_{34} t_{sub}(t_b + t_{ch})\right]} - 2\varphi_1(x, -t_p) - \left(\left.\frac{\partial^2 \varphi_1(x, y)}{\partial y^2}\right|_{y=-t_p}\right) \times \frac{\left(K_{14} t_{sub} t_p + t_p^2 + 2K_{12} t_{ch} t_p + 2K_{34} t_b t_p\right)}{\left[(t_b + t_{ch})^2 + K_{34} t_{sub}(t_b + t_{ch})\right]} \tag{A17}$$

Here, same as that in conventional derivation process of silicon lateral power device, a characteristic thickness $t = [0.5(t_b+t_{ch})^2+0.5K_{34}t_{sub}(t_b+t_{ch})]^{0.5}$ can be defined to simplify the following derivation process. Further, by subsisting

Eq. (A7) to Eq. (A1) and (A2), respectively, the following equation can be obtained accordingly:

$$\left.\frac{\partial^2\varphi_1(x,y)}{\partial y^2}\right|_{y=-t_p} - \left.\frac{\partial^2\varphi_2(x,y)}{\partial y^2}\right|_{y=0} = -\frac{qN_1}{\varepsilon_1} + \frac{qN_2}{\varepsilon_2} \quad \text{(A18)}$$

By using the Eq. (A18) and (A17), the Eq. (A1) can be re-written as:

$$\left.\frac{\partial^2\varphi_1(x,y)}{\partial y^2}\right|_{y=-t_p} = -\frac{2\varphi_1(x,-t_p)}{K_{14}t_{sub}t_p + t_p^2 + 2K_{12}t_{ch}t_p + 2K_{34}t_bt_p} + \left(\frac{qN_2}{\varepsilon_2} - \frac{qN_3}{\varepsilon_3}\right)\left(\frac{t_b + K_{34}t_bt_{sub}}{K_{14}t_{sub}t_p + t_p^2 + 2K_{12}t_{ch}t_p + 2K_{34}t_bt_p}\right) + \left(\frac{qN_2}{\varepsilon_2} - \frac{qN_1}{\varepsilon_1}\right)\left(\frac{2t^2}{K_{14}t_{sub}t_p + t_p^2 + 2K_{12}t_{ch}t_p + 2K_{34}t_bt_p}\right) - \left(\frac{V_{2DEG}}{t_{pas}}\right)\left(\frac{K_{14}t_{sub} + 2t_p + 2K_{12}t_{ch} + 2K_{13}t_b}{K_{14}t_{sub}t_p + t_p^2 + 2K_{12}t_{ch}t_p + 2K_{34}t_bt_p}\right) \quad \text{(A19)}$$

Since the t_p is relatively small compared to the channel or buffer layer thickness and N_1 is also negligible when compared to the charge density of 2DEG, it is reasonable to recognize that the barrier layer itself scarcely contributes to the devices' off-state breakdown characteristics. The simulation results indicate the same conclusion. Therefore, in the proposed model, by neglecting the N_1 and t_p, the 2-D Poisson equation in channel layer can be further simplified as:

$$\frac{\partial^2\varphi_1(x,-t_p)}{\partial x^2} + \left.\frac{\partial^2\varphi_2(x,y)}{\partial y^2}\right|_{y=0} = -\frac{qN_2}{\varepsilon_2},\ y=0 \quad \text{(A20)}$$

By subsisting Eq. (A18), (A12) and (A7) to (A20), a general differential equation for the surface potential of the channel layer, namely Eq. (5) can be therefore obtained. Worthy of note is that the derivation of Eq. (5) in the Appendix only provides the main steps. The idea of derivation is to use the transitivity of boundary conditions and Poisson's equation to gain enough boundary conditions for each semiconductor layer for modeling, especially the channel layer.

2. The physics model and setting of traps in each layer and interface used in Sentaurus simulation:

For both the buffer, channel and AlGaN layers, the physics models for recombination are SRH and Radiative.

For the buffer layer, the traps are set as acceptor whose concentration is $1.0 \times 10^{17}\text{cm}^{-3}$. The energy location of traps is 0.6eV above the middle of bandgap. The traps at GaN/Silicon interface are set as acceptor whose concentration is $5.0 \times 10^{13}\text{cm}^{-3}$. The energy location of traps is 1.2eV above the middle of the bandgap. For the channel layer, the traps are set as acceptor whose concentration is $1.0 \times 10^{16}\text{cm}^{-3}$. The energy location of traps is 0.4eV above the middle of the bandgap. For the AlGaN layer, the traps are set as acceptor whose concentration is $1.0 \times 10^{17}\text{cm}^{-3}$. The energy location of traps is 0.4eV above the middle of the bandgap. The traps at AlGaN/Si_3N_4 interface are set as donor whose concentration is $5.0 \times 10^{13}\text{cm}^{-3}$. The energy location of traps is 0.4eV under the middle of bandgap.

REFERENCES

[1] C. Yang *et al.*, "AlGaN/GaN MIS-HEMT with AlN interface protection layer and trench termination structure," *IEEE Trans. Electron Devices*, vol. 65, no. 11, pp. 5203–5207, Nov. 2018, doi: 10.1109/TED.2018.2868104.

[2] R. Zhu *et al.*, "A split gate vertical GaN power transistor with intrinsic reverse conduction capability and low gate charge," in *Proc. IEEE Int. Symp. Power Semicond. Devices ICs (ISPSD)*, Chicago, IL, USA, 2018, pp. 212–215, doi: 10.1109/ISPSD.2018.8393640.

[3] K. J. Chen *et al.*, "GaN-on-Si power technology: Devices and applications," *IEEE Trans. Electron Devices*, vol. 64, no. 3, pp. 779–795, Mar. 2017, doi: 10.1109/TED.2017.2657579.

[4] J. Zhang *et al.*, "One-dimensional breakdown voltage model of SOI RESURF lateral power device based on lateral linearly graded approximation," *Chin. Phys. B*, vol. 24, Feb. 2015, Art. no. 028502, doi: 10.1088/1674-1056/24/2/028502.

[5] M. Imam, M. Quddus, J. Adams, and Z. Hossain, "Efficacy of charge sharing in reshaping the surface electric field in high voltage lateral RESURF devices," *IEEE Trans. Electron Devices*, vol. 51, no. 1, pp. 141–148, Jan. 2004, doi: 10.1109/TED.2003.821383.

[6] J. Zhang *et al.*, "A new physical insight for the 3-D-layout-induced cylindrical breakdown in lateral power devices on SOI substrate," *IEEE Trans. Electron Devices*, vol. 65, no. 5, pp. 1843–1848, May 2018, doi: 10.1109/TED.2018.2810325.

[7] P. Srivastava *et al.*, "Record breakdown voltage (2200 V) of GaN DHFETs on Si with 2-um buffer thickness by local substrate removal," *IEEE Electron Device Lett.*, vol. 32, no. 1, pp. 30–32, Jan. 2011, doi: 10.1109/LED.2010.2089493.

[8] P. Srivastava, J. Das, R. P. Mertens, and G. Borghs, "Silicon substrate engineered high-voltage high-temperature GaN-DHFETs," *IEEE Trans. Electron Devices*, vol. 60, no. 7, pp. 2217–2223, Jul. 2013, doi: 10.1109/TED.2013.2263253.

[9] N. Herbecq *et al.*, "900 V, 1.6 mΩ cm^2 AlN/GaN-on-Si power devices realized by local substrate removal," *Appl. Phys. Exp.*, vol. 7, no. 3, Art. no. 034103, 2014, doi: 10.7567/apex.7.034103.

[10] N. Herbecq *et al.*, "Above 2000 V breakdown voltage at 600 K GaN-on-silicon high electron mobility transistors". *Phys. Status Solidi A*, vol. 213, no. 4, pp. 873–877, 2016, doi: 10.1002/pssa.201532572.

[11] Y.-F. Wu *et al.*, "30-W/mm GaN HEMTs by field plate optimization," *IEEE Electron Device Lett.*, vol. 23, no. 3, pp. 117–119, Mar. 2004, doi: 10.1109/LED.2003.822667.

[12] J. Zhang, Y.-F. Guo, and D. Z. Pan, "Role of shape factor in forming surface electric field basin in RESURF lateral power devices and its optimization design," *IEEE J. Electron Devices Soc.*, vol. 6, pp. 1147–1153, Sep. 2018, doi: 10.1109/JEDS.2018.2871505.

[13] S. Karmalkar, J. Deng, and M. S. Shur, "RESURF AlGaN/GaN HEMT for high voltage power switching," *IEEE Electron Device Lett.*, vol. 22, no. 8, pp. 373–375, Aug. 2001, doi: 10.1109/55.936347.

[14] Z. Zhao, Z. Zhao, Q. Luo, and J. Du, "High-voltage RESURF AlGaN/GaN high electron mobility transistor with back electrode," *Electron. Lett.*, vol. 49, no. 25, pp. 1638–1640, May 2013, doi: 10.1049/el.2013.3366.

[15] G. Sabui and Z. J. Shen, "Analytical calculation of breakdown voltage for dielectric RESURF power devices," *IEEE Electron Device Lett.*, vol. 38, no. 6, pp. 767–770, Jun. 2017, doi: 10.1109/LED.2017.2690964.

[16] L. Yang, B. Duan, Y. Wang, and Y. Yang, "Analytical models for the electric field and potential of AlGaN/GaN HEMT with partial silicon doping," *Superlattices Microstruct.*, vol. 128, pp. 349–357, Apr. 2019, doi: 10.1016/j.spmi.2019.02.010.

[17] G. Haijun, D. Baoxing, W. Hao, and Y. Yintang, "Analytical model of AlGaN/GaN HEMTs with a partial GaN cap layer," *Superlattices Microstruct.*, vol. 128, pp. 210–217, Nov. 2018, doi: 10.1016/j.spmi.2018.07.031.

[18] J. A. Appels and H. M. J. Vaes, "High voltage thin layer devices (RESURF devices)," in *Int. Electron Devices Meeting (IEDM) Tech. Dig.*, 1997, pp. 238–241, doi: 10.1109/IEDM.1979.189589.
[19] G. Ghione, "Looking for quality in TCAD-based papers," *IEEE Trans. Electron Devices*, vol. 66, no. 8, pp. 3252–3253, Aug. 2019, doi: 10.1109/TED.2019.2924360.

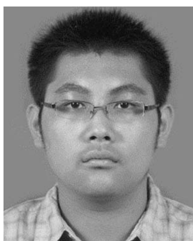

JUN ZHANG (Member, IEEE) received the Ph.D. degree in microelectronics from the Nanjing University of Posts and Telecommunications, Nanjing, China, in 2018, where he is currently a Postdoctoral Scholar with the College of Electronic and Optical Engineering. His current research interests include semiconductor power devices, microelectronics devices reliability, and RF and power integrated circuits and systems.

YUFENG GUO (Member, IEEE) received the Ph.D. degree in microelectronics and solid-state electronics from the University of Electronic Science and Technology of China, Chengdu, China, in 2005. He is the Dean of the College of Electronic and Optical Engineering and the Vice-Director of the National and Local Joint Engineering Laboratory of RF Integration and Micro-Assembly Technology, NJUPT. He has published about more than 180 articles in refereed journals and conferences and holding over 20 Chinese patents.